

Hydrogenolysis of lignin model compounds into aromatics with bimetallic Ru-Ni supported onto nitrogen-doped activated carbon catalyst



Yinghui Hu¹, Guangce Jiang¹, Guoqiang Xu*, Xindong Mu*

CAS Key Laboratory of Bio-based Materials, Qingdao Institute of Bioenergy and Bioprocess Technology, Chinese Academy of Sciences, Qingdao, Shandong, 266101, PR China

ARTICLE INFO

Article history:

Received 20 June 2017

Received in revised form

29 November 2017

Accepted 7 December 2017

Available online 22 December 2017

Keywords:

Hydrogenolysis

Lignin model compounds

Bimetallic catalyst

Nitrogen-doped

Synergistic effects

ABSTRACT

Lignin is the most abundant and renewable resources for production of natural aromatics. In this paper, new bimetallic catalytic system of Ru and Ni supported onto nitrogen-doped activated carbon (Ru-Ni-AC/N) was developed and its performances on hydrogenolysis of lignin model compounds under mild reaction conditions (1.0 MPa, 230 °C, in aqueous) were investigated. The results indicate that Ru-Ni-AC/N was a highly active, selective and stable catalyst for the conversion of lignin model compounds into aromatics, e.g. phenol, benzene and their derivatives. As verified by BET, XRD, HRTEM, XPS, H₂-TPR and ICP-MS, the strong synergistic effects between i) Ru and Ni and ii) metals and N-groups were contributed to its excellent aromatics selectivity. What's more, the introduction of electron rich N atoms on AC was beneficial to the stabilization of metal particles, which greatly enhanced the durability of the catalyst.

© 2017 Published by Elsevier B.V.

1. Introduction

Lignin is a natural polymer of methoxylated phenylpropane units and holds considerable potential as a renewable resource for the sustainable production of fuels and bulk chemicals [1,2]. Via fast pyrolysis process, it can be converted into a liquid mixture, which containing about 5–35% of phenolic chemicals [3]. Those phenols can be a potential feedstock to produce aromatics, e.g. phenol, benzene and their derivatives, instead of petrochemical resource via hydrogenolysis. Besides solvents, these aromatic compounds are basic feedstock in multiple chemical processes, which are more economical variable than normal biofuels [4]. Especially, phenol and its derivatives are widely used as chemical building blocks for synthetic bioplastics. As shown in **Scheme 1**, there is generally a competition between hydrogenolysis and hydrogenation of guaiacol [5–9] during the catalytic process. Therefore, the selective cleavage of C–O bonds without aromatic ring hydrogenation is of great importance.

Previous works revealed that noble metals such as Pd, Pt, Ru and Rh, offer high activities for hydrogenolysis reactions, but they

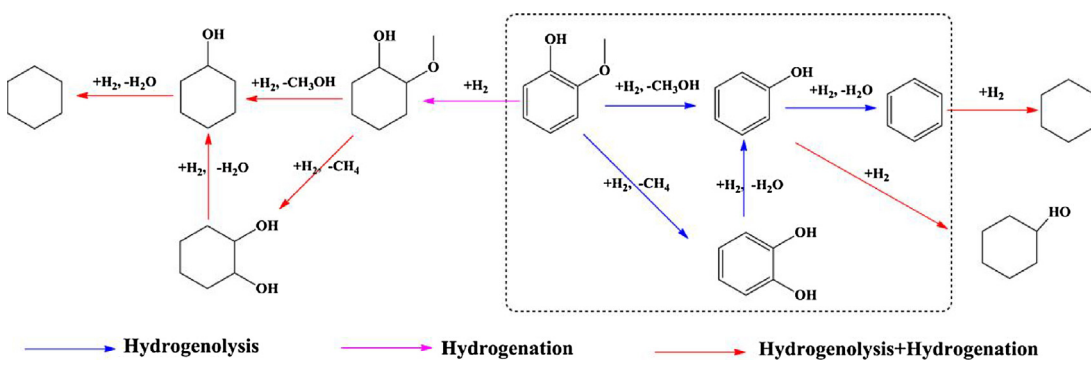
are also highly active for hydrogenation of aromatic rings to produce cycloparaffin [10–12]. Non-noble transition metals, such as Ni and Fe, display low activity for hydrogenation reactions but high selectivity for aromatic rings [13–15]. Hong et al. [16] synthesized a series of Pd-Fe₂O₃ catalysts and applied them for hydrogenolysis of m-cresol. They found that the addition of Pd remarkably promoted the catalytic activity and showed high selectivity towards toluene without saturation of aromatic ring and C–C cleavage. What's more, the combination of Fe with Pd supported onto activated carbon (Pd-Fe-AC) could enhance the benzene yield dramatically compared with Fe-AC and Pd-AC during the process of vapor-phase guaiacol hydrogenolysis reaction [17].

Although activated carbon is the most potential “sustainable” host materials for metal particles, the metals deposited on carbons can be easily leached during catalytic processes owing to the weak interaction between the metals and the carbon surface [18]. Nitrogen doping was proved to be an efficient strategy to modify the surface and physicochemical properties of activated carbon support [19]. Xu et al. [20] have synthesized palladium nanoparticles supported on mesoporous nitrogen-doped activated catalyst (Pd-AC/N) and have tested its catalytic ability for biofuel upgrade. The high catalytic performance of catalyst was attributed to the special structure of nitrogen-doped activated carbon and metal heterojunction which leads to a very stable and uniform dispersion of Pd

* Corresponding authors.

E-mail addresses: xugq@qibebt.ac.cn (G. Xu), muxd@qibebt.ac.cn (X. Mu).

¹ These authors contributed equally.

**Scheme 1.** Cleavage of C—O bonds and hydrogenation of aromatic ring.

nanoparticles. It was also evidenced by our previous work [21] that the stability of Ir-AC/N catalyst improved a lot compared with Ir-AC, on account of the interaction between N-groups and Ir particles.

In this study, a novel kind of catalysts were prepared by loading Ru and Ni on nitrogen-doped activated carbon (AC/N), and their performances in hydrogenolysis of lignin based monomeric substrates (guaiacol, alkyl substituted guaiacol, syringol, etc.) were tested under mild reaction conditions (1.0 MPa, 230 °C, in aqueous). The influence of major reaction parameters, such as metal loading, H₂ pressure, reaction temperature and solvent, were fully investigated and the possible reaction pathways were also proposed. Moreover, the interaction among Ru, Ni and the electron rich N atoms were analyzed in detail by BET, XRD, HRTEM, H₂-TPR, XPS and ICP-MS to dissect the good aromatics yield and enhanced durability of the new catalyst.

2. Experimental

2.1. Materials

Commercially available chemicals including metal precursors of Ru, Ni, Pt and Fe, 1,10-phenanthroline, lignin phenolic model compounds and other organic reagents were purchased from SCRC, Alfa Aesar or TCI and used as received. Activated carbon support (Vulcan XC72R) was provided by Cabot Corporation.

2.2. Catalyst preparation

2.2.1. The preparation of AC/N support

The AC/N support were prepared according to reference [21]. Generally, 5 g 1,10-phenanthroline monohydrate was dissolved in 25 mL ethanol, and then mixed slowly with aqueous solution of H₂SO₄ (5 g 98% H₂SO₄ diluted with 25 mL deionized water). Ethanol and water were removed by distillation after the mixture stirred for 4 h. Followed, 2.5 g of the synthesized phenanthroline sulfuric acid salt, 5 g activated carbon (Vulcan XC72R), 80 mL of deionized water and 50 mL of ethanol were added into a 250 mL round-bottom flask and stirred at room temperature for 12 h. After all solvents were evaporated, the obtained black solids were calcined at 900 °C in a tube furnace under N₂ atmosphere for 6 h with a heating rate of 5 °C min⁻¹. Finally, the nitrogen-doped activated carbon support was obtained.

2.2.2. The preparation of mono- and bi- metallic catalysts

All catalysts were prepared by incipient wetness impregnation method. Chloride nickel hydrate (NiCl₂·6H₂O), rhodium chloride hydrate (RuCl₃·6H₂O), palladium chloride hydrate (PdCl₂·H₂O), iron chloride hydrate (FeCl₃·6H₂O), and activated carbon (AC), nitrogen-doped activated carbon (AC/N) were used as metal precursors and supports, respectively. Take 1%Ru-5%Ni-AC/N as an

example, 0.02 g RuCl₃·3H₂O and 0.15 g NiCl₂·6H₂O were dissolved into 5 mL water, then 0.75 g nitrogen-doped carbon support was added into the solution with stirring for 5 h at room temperature. After that, water was removed by a rotary evaporator and the obtained powder was dried at 110 °C overnight. The dried samples were reduced in a H₂ flow at 200 °C for 5 h prior to use. The obtained catalyst was denoted as x%Ru-y%Ni-AC/N, where x% and y% refer to the mass percentage of Ru and Ni.

2.3. Catalyst characterization

BET (Brunauer-Emmett-Teller) and Barrett-Joyner-Halenda (BJH) were conducted using an ASAP-2020 analyzer. XRD (Powder X-ray diffraction) was recorded at a Bruker D8 diffractometer with Cu target and K α ($\lambda = 1.54 \text{ \AA}$) radiation. HRTEM (High-resolution transmission electron microscopy) images were performed with FEI Tecnai G20 instrument. EDS elemental mappings were carried out on Hitachi SU8000 instrument and XEDS elemental analyses were performed with JEM-2100F electron microscope which equipped with an Oxford X-MaxN80T energy dispersive X-ray spectroscopy. The XEDS elemental analyses were tested by controlling the position of irradiated area within 5 nm. During TEM samples prepared, the powder samples were dissolved in ethanol under ultrasonication for 5 min, and then several droplets of the sample were laid on a copper grid coated with carbon film.

The XPS (X-ray photoelectron spectroscopy) spectra were performed with a Thermo Escalab 250XI system using an Al K α (1486.6 eV) as the X-ray source and deconvoluted with XPS PEAK41 software. The binding energies were calibrated using a criterion of C 1 s peak (284.8 eV) as a reference.

H₂-TPR (H₂-temperature programmed reduction) was carried out on a Chemisorption Analyzer (Micromeritics AutoChem II 2920) equipped with a thermal conductivity detector (TCD). For H₂-TPR analysis, about 100 mg of sample was used for each measurement and pre-treated in a Ar flow at 200 °C for 2 h. TPR was initiated from room temperature to 900 °C at 10 °C min⁻¹ with a mixture flow of 10% H₂/Ar (20 mL min⁻¹).

ICP-MS (inductively coupled plasma mass spectrometry) was performed on an Agilent 7700ce system. After each reaction, the aqueous solution was diluted with water to 100.0 mL prior to subject to the analyzer.

For H₂-TPD (H₂-temperature programmed desorption) analyses, Micromeritics AutoChem II 2920 Chemisorption Analyzer was used as instrument. The sample (100 mg) was pre-treated under Ar flow at 300 °C for 2 h, and then cooled to 230 °C for 2 h. After exposed to a 10% H₂/Ar flow (20 mL min⁻¹), the physical adsorption of H₂ was purged by Ar flow for 2 h until pulses base line became stable. Furnace temperature was increased from 100 to 800 °C with a heating rate of 10 °C min⁻¹ in a Ar flow.

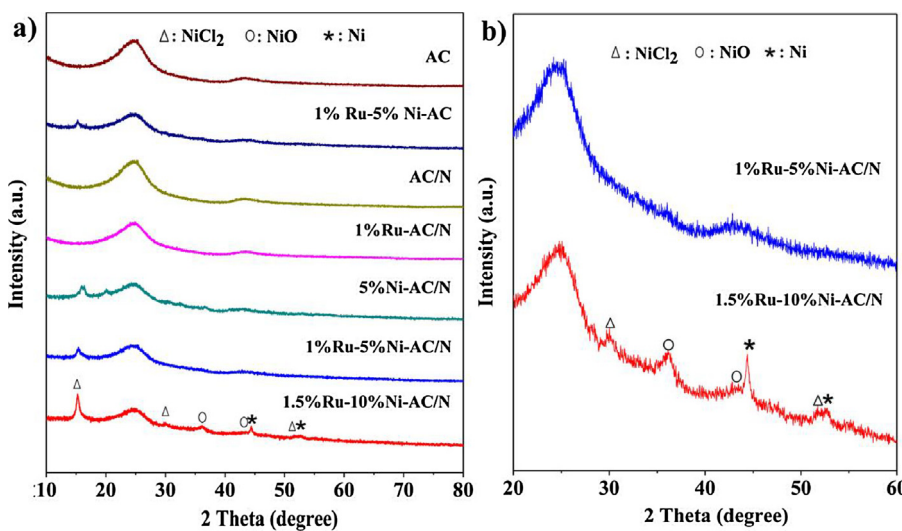


Fig. 1. a) XRD patterns of the catalysts and b) partial patterns ($20\text{--}60^\circ$) of 1%Ru-5%Ni-AC/N and 1.5%Ru-10%Ni-AC/N catalyst.

2.4. Catalytic activity test

In a typical experiment, the reactant, solvent and catalysts were charged into a 100 mL autoclave equipped with a magnetic stirrer. After purging the reactor with hydrogen 3 times to remove the air, the reactor was charged with the desired H_2 pressure and heated to the reaction temperature. When the reaction was finished, the reactor was quickly cooled by cold water to minimize the by-products. The products were extracted by 25 mL ethyl acetate and subsequently analyzed by GC (Shimadzu, GC-2010 Plus) and GC-MS (Shimadzu, GCMS-QP 2010 Ultra). N-dodecane was used as an internal standard. Conversion (Con.%), selectivity to aromatics (S-a.%) and yield were calculated according to the following equations:

$$\text{Con.}\% = \left(1 - \frac{n_{\text{rea}}^c}{n_{\text{rea}}^i} \right) \times 100\%$$

$$S_{\text{-a.}}\% = \left(\frac{n_{\text{phe}}^c + n_{\text{ben}}^c}{n_{\text{rea}}^i - n_{\text{rea}}^c} \right) \times 100\%$$

$$\text{Yield} = \text{Con.}\% \times S_{\text{-a.}}\% \div 100\%$$

Where n^i and n^c are the initial and current mole number; the subscripts “rea”, “phe”, “are” were used to denote the reactant, generated phenol (phenol derivatives) and generated benzene (benzene derivatives), respectively.

3. Results and discussion

3.1. Physicochemical properties

The BET surface area of the activated carbon (AC) was ca. $220\text{ m}^2/\text{g}$. To estimate the influence of acid conditions during preparation of N-doped AC, acid treated AC without N-doping and metal loading was also discussed. After acid treatment and loading with N-groups and metals, decrease on BET surface area and increase on average pore diameter were found in all samples as excepted (Table 1). Such phenomenon clearly indicated that existing acid during N-groups loading could collapsed the adjacent pore walls, N-groups and metal particles blocked some small diameter pores, all of which resulted in wider pores and smaller BET surface area of the carbon support [22,23].

Table 1
Pore structure parameters of catalysts tested by N_2 adsorption-desorption.

Sample	BET surface area (m^2/g)	Average pore diameter (4 V/A) (nm)
AC	220.25	11.65
AC(Acid Treated ^a)	185.32	18.47
1%Ru-5%Ni-AC	180.17	13.45
AC-N	173.21	21.50
1%Ru-AC/N	167.91	18.32
5%Ni-AC/N	155.49	16.12
1%Ru-5%Ni-AC/N	155.46	20.38
1.5%Ru-10%Ni-AC/N	133.58	21.57
1%Ru-5%Ni-AC/N (recycle 3 times)	145.08	21.23

^a Acid treated processes were: 2.5 g purchased AC was added into a H_2SO_4 solution (water/ethanol, 40 mL/25 mL) with the pH of ca. 4.0, which was similar to the pH of phenanthroline sulfuric acid salt solution. After stirred at room temperature for 12 h and evaporated all solvent, the obtained black solids were calcined at 900°C under N_2 atmosphere for 6 h and reduced at 200°C under H_2 atmosphere for 5 h.

The XRD patterns of the prepared catalysts were present in Fig. 1. The broad peak at $20\text{--}30^\circ$ was attributed to amorphous AC and AC/N support [24]. When 1 wt.% or 1.5 wt.% content of Ru was deposited on AC/N (1%Ru-AC/N or 1%Ru-5%Ni-AC/N or 1.5%Ru-10%Ni-AC/N), there was no obvious change observed. However, when 5 wt.% Ni content was loaded (5%Ni-AC/N or 1%Ru-5%Ni-AC/N), new diffraction peak corresponding to NiCl_2 was found at 15.3° , indicating Ni^{2+} was not completely reduced to Ni^0 by H_2 during the catalysts preparation process. When Ni loading content was increased to 10 wt.%, new diffraction peaks at 44.7° and 53.5° related to metallic Ni and 36.8° and 43.5° to NiO gradually showed up (1.5%Ru-10%Ni-AC/N). The presence of NiO phase indicating the reduced Ni was oxidized by O_2 in air. The undetectable peaks of Ru and/or Ni species in samples of 1%Ru-AC/N, 5%Ni-AC/N, 1%Ru-5%Ni-A/N and 1%Ru-5%Ni-AC were resulted from the low content and the well dispersed nano metallic and metallic oxide particles on the supports, which can be confirmed by the HRTEM and corresponding EDS elemental mappings (Fig. 2). From Fig. 2a-f, metallic and metallic oxide particles were partially dispersed on the spherical supports in the size range from 0.5 to 2 nm. Both Ni and Ru were found within 5 nm indicating that two metals coexisted in close distances as testified by HRTEM-XEDS elemental analyses (Fig. 3). EDS elemental mappings proved that the location region of Ru did not overlap that of Ni suggesting majority of Ru-Ni coexisted in the form of separate particles with close distance [25], which was in accordance with the work of Lucília S. Ribeiro et al. [26]. Morales-

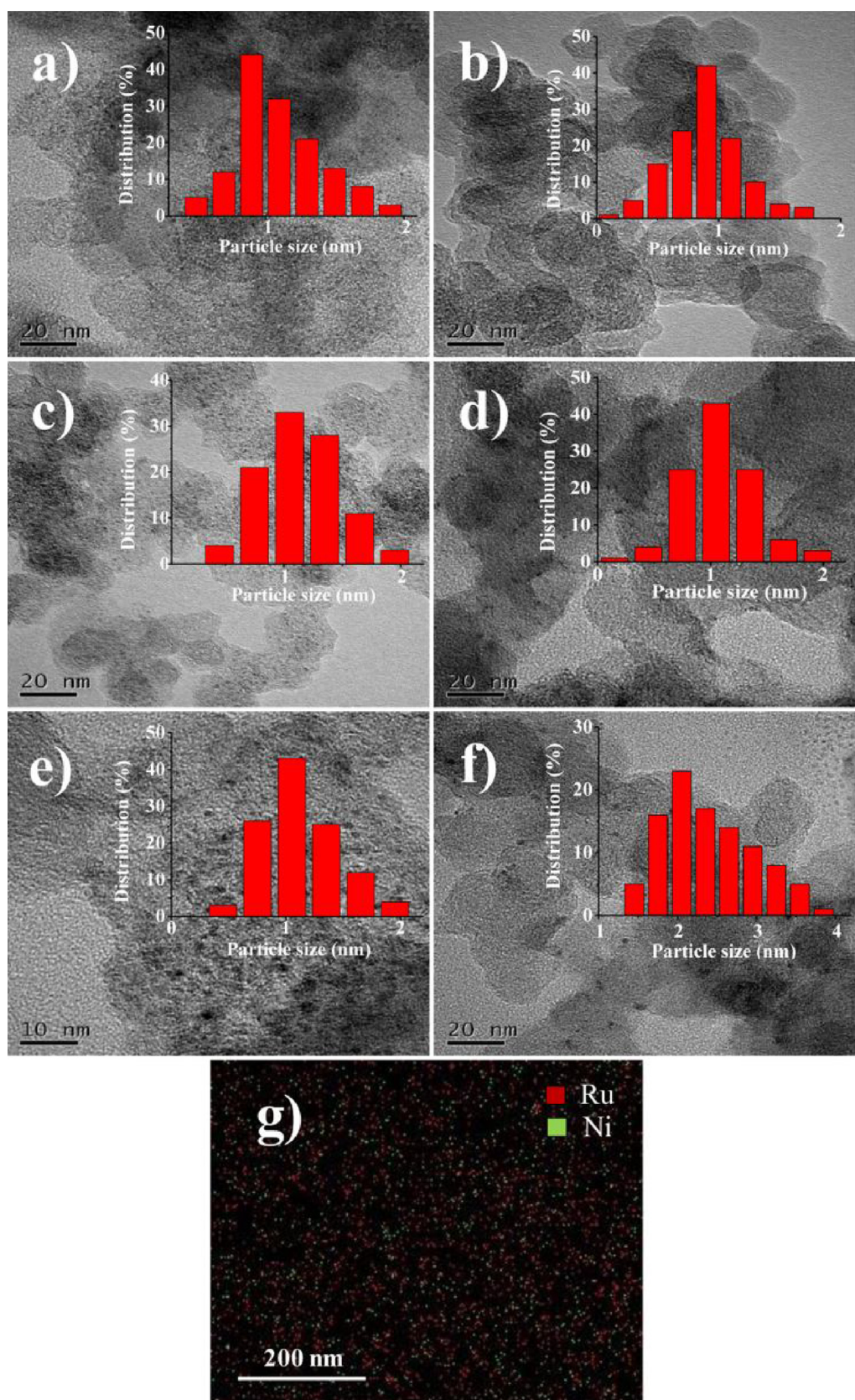


Fig. 2. HRTEM of the supported catalysts with a) 1%Ru-AC/N, b) 5%Ni-AC/N, c) 1%Ru-5%Ni-AC/N, d) 1%Ru-5%Ni-AC, e) 1.5%Ru-10%Ni-AC/N, f) 1%Ru-5%Ni-AC/N(recycle 3 times) and g) EDS elemental mappings of Ru (red) and Ni (green) in 1%Ru-5%Ni-AC/N catalyst. (For interpretation of the references to colour in this figure legend, the reader is referred to the web version of this article.)

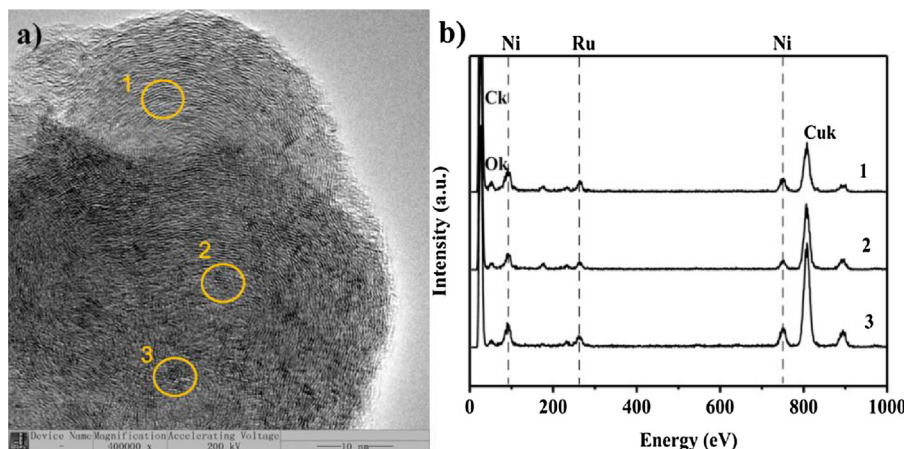


Fig. 3. a) HRTEM image and b) XEDS elemental analyses of the 1%Ru-5%Ni-AC/N catalyst.

Table 2

Catalytic performance of prepared catalysts for hydrogenolysis of guaiacol.^a

Entry	Catalyst	Yield (%)	Con. (%)	S-a (%)	Selectivity (%)				
					1	2	3	4	5
1	AC	— ^b	—	—	—	—	—	—	—
2	AC/N	—	—	—	—	—	—	—	—
3	1%Ru-AC/N	8	74	11	2	9	1	50	38
4	5%Ni-AC/N	—	—	—	—	—	—	—	—
5	1%Ru-5%Ni-AC/N	57	69	83	24	59	1	10	6
6	1%Ru-AC/N+5%Ni-AC/N ^c	14	71	20	5	15	1	58	21
7	1%Ru-5%Ni/AC	40	63	64	19	45	2	24	10
8	1%Ru-5%Fe-AC/N	32	40	80	23	57	3	5	12
9	1%Pd-5%Fe-AC/N	17	33	51	14	37	12	14	23
10	1%Pd-5%Ni-AC/N	19	39	48	13	35	6	23	23

^a Reaction conditions: guaiacol 6.0 mmol, catalyst 0.1 g, H₂O 35 mL, 230 °C, H₂ 1.0 MPa, 4 h.

^b ‘—’ means no product or only a trace amount of product was obtained.

^c The two catalysts were all 0.1 g.

Cano et al. also concluded that only very small Ru-Ni alloy formed and the majority of the Ni and Ru existed in the form of nearly monometallic particles as verified by EXAFS analysis [27].

XPS characterizations were employed to investigate the surface valence state of the catalysts, as shown in Fig. 4. For 1%Ru-AC/N (Fig. 4a), the intense doublet peaks of 3p_{3/2} and 3p_{1/2} for Ru (0) appeared at 462.5 and 484.9 eV, while the weak 3p_{3/2} and 3p_{1/2} peaks appeared at 464.5 and 487.3 eV are attributed to RuCl₃, and peak at 467.2 and 489.6 eV are assigned to RuO₂ [28]. Ru 3p was also exhibited satellite structure peak at 474.0 eV. For 5%Ni-AC/N (Fig. 4b), two peaks centered at 856.3 and 874.0 eV are corresponding to metallic Ni 2p_{3/2} and 2p_{1/2}, and peaks with binding energies of 862.0 and 880.8 eV indexed to Ni²⁺ (NiCl₂, NiO) 2p_{3/2} and 2p_{1/2} have also been detected [29,30].

An obvious shift of Ru 3p and Ni 2p peak to higher binding energy (about 0.2–0.8 eV) were observed (Fig. 4a, b) when Ru and Ni were supported together on AC/N(1%Ru-5%Ni-AC/N), indicating there was indeed a synergistic effect between Ru and Ni. Owing to a strong interaction effect between metals and N-groups, peaks of Ru and Ni for Ru-Ni-AC/N catalyst were shifted to higher binding energy (about 0.2–0.6 eV) when compared with Ru-Ni-AC (Fig. 4a, b).

The 1%Ru-5%Ni-AC/N catalyst had a nitrogen content of 1.5 atomic% as measured by XPS, suggesting N-groups were doped suc-

cessfully in the activated carbon catalysts. Fig. 4 (c) shows XPS spectrum of N 1s and the two N 1s peaks were corresponded to pyridinic nitrogen (398.8 eV) and graphitic nitrogen (402.2 eV). The pyridinic-N was the major species that enhanced the binding between metal NPs and N-doped AC support because their lone pair electrons can serve as metal coordination sites [31,32].

The H₂-TPR spectra of the catalysts were presented in Fig. 5. A H₂ consumption zone at 450–750 °C was detected for both AC and AC/N supports, which was mainly caused by the reduction of functional groups on the support [33]. For 1%Ru-AC/N, a peak at 176 °C appeared together with a weak shoulder peak at 335 °C, which were attributed to the reduction of RuCl₃ and RuO₂ [33], respectively. 5%Ni-AC/N presented a main hydrogen consumption peak at 370 °C belonging to the Ni²⁺ (NiCl₂, NiO) reduction peak [34]. For 1%Ru-5%Ni-AC/N bimetallic catalyst, the reduction peak of RuCl₃ and RuO₂ was at 176 °C unchanged, while the hydrogen consumption peaks corresponding to the reduction of Ni²⁺ (NiCl₂, NiO) was shifted towards a lower reduction temperature (305 °C). Those results also implied the synergistic effect existed between Ru and Ni. The addition of ruthenium metal site could enhance the splitting of more molecular hydrogen into atomic hydrogen, and Ni²⁺ cations are more rapidly reduced by atomic hydrogen than by molecular hydrogen [35,36]. Compared with 1%Ru-5%Ni-AC/N, the reduction peaks of RuCl₃, RuO₂, NiCl₂ and NiO in 1%Ru-5%Ni-AC

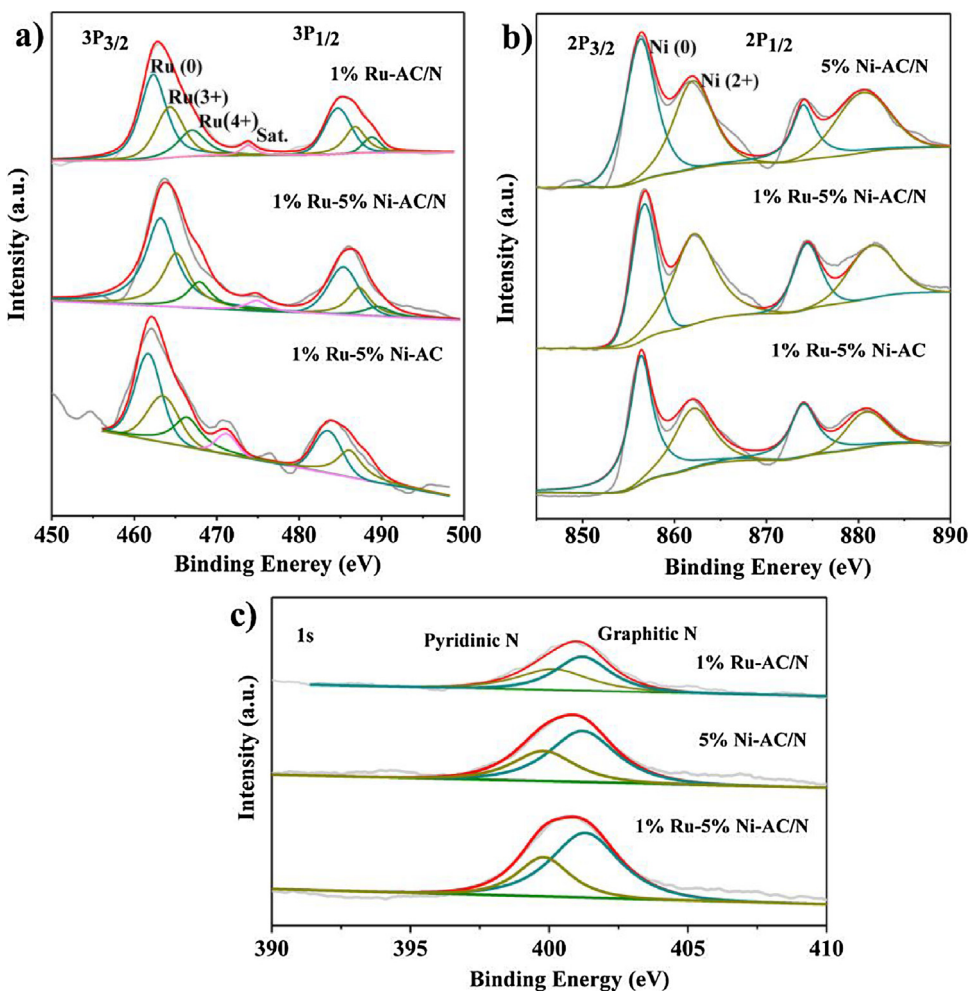


Fig. 4. XPS comparison of various catalysts with a) Ru 3p XPS, b) Ni 2p XPS and c) N 1s XPS.

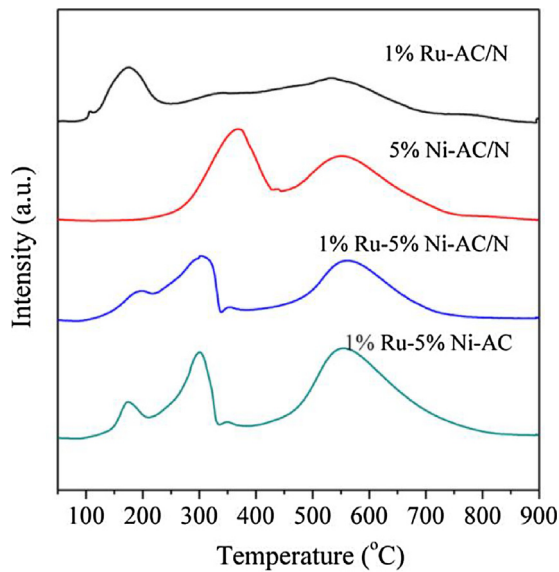


Fig. 5. $\text{H}_2\text{-TPR}$ spectra of the catalysts.

shift to lower temperature of 170 °C and 300 °C, indicating that the Ru³⁺(RuCl₃), Ru⁴⁺(RuO₂) and Ni²⁺ (NiCl₂, NiO) in 1%Ru-5%Ni-AC/N have been both stabilized by the N atoms.

3.2. Catalytic activity

The performances of different catalysts for the hydrogenolysis of guaiacol were listed in Table 2. GC-MS analysis revealed that the products were benzene, phenol, cyclohexane, cyclohexanol and the others (2-methoxy cyclohexanol and trace amount of the carbon loss).

The blank supports AC and AC/N showed no catalytic activity (Table 2, entries 1, 2). When 1 wt.% of Ru was loaded on AC/N (1%Ru-AC/N), the conversion was enhanced dramatically to 74%, and most of the benzene rings were fully saturated owing to the excellent hydrogenation ability of Ru (Table 2, entry 3). On the other hand, 5%Ni-AC/N displayed no catalytic activity under such mild conditions (Table 2, entry 4) [16,37]. However, when 1%Ru-5%Ni-AC/N was used as catalyst, the yield of aromatics was dramatically increased from 8% to 57% (Table 2, entries 3–5). Those result implied that the synergistic effects between Ru and Ni, which certificated by HRTEM, XPS and H₂-TPR, could enhance the selectivity towards aromatic products. To further confirm this conclusion, 1%Ru-AC/N and 5%Ni-AC/N were mechanically mixed to catalyze this reaction and only 14% of aromatics yield was obtained (Table 2, entry 6).

To investigate the influence of N functionalized carbon supports, non N functionalized activated carbon support catalyst 1%Ru-5%Ni-AC were prepared. As shown in Table 2 (entries 5 and 7), AC supported catalyst showed a lower conversion (63%) and selectivity (64%) compared with AC/N supported catalyst (69% and 83%).

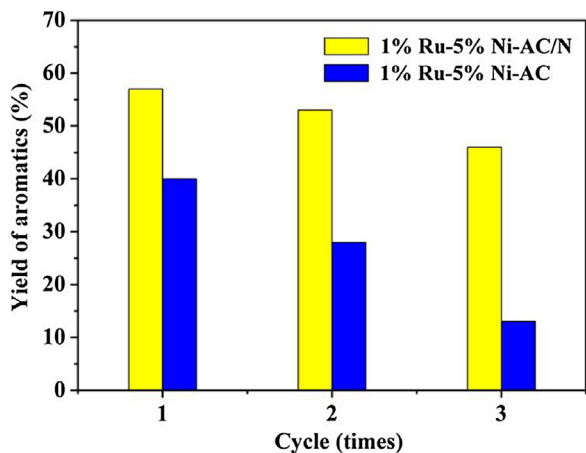


Fig. 6. The performance of Ru-Ni-AC/N and Ru-Ni-AC catalysts on guaiacol hydrogenolysis reaction for 3 recycles.

Apart from Ru and Ni, Pd and Fe were also chosen as candidates for this hydrogenolysis reactions because previous report [17] suggested that Pd-Fe was efficient for catalyzing vapor-phase guaiacol hydrogenolysis reaction. However, the results (Table 2, entries 8–10) indicated that the combination of Pd-Fe, Pt-Ni and Ru-Fe showed less activity than Ru-Ni for guaiacol hydrogenolysis conversion under the mild reaction conditions.

3.3. The recycling property of catalyst

For testing the stability of the supported catalysts, Ru-Ni-AC/N catalyst was recycled. Non-nitrogen-doped Ru-Ni-AC catalyst was also measured for contrast. The catalysts was recovered by filtration, washed by deionized water, dried 12 h at 110 °C and then reduced 4 h in H₂ at 200 °C after each reaction run. After three recycles, Ru-Ni-AC/N catalyst retained 80% of the original activity (Fig. 6). However, Ru-Ni-AC catalyst only showed 40% of the original activity, which was far lower than the Ru-Ni-AC/N catalyst (Fig. 6). The loss of activity was probably caused by the leaching of metal particles (Table 3), metal aggregation (Fig. 2f) and possible metal oxidation.

The leaching of Ru and Ni of Ru-Ni-AC/N catalyst were analyzed by ICP-MS (Table 3). Although metals leaching was found in both catalysts to varying degrees, the amount of metal leaching in N-doped AC was much less than that in non-N doped AC. Compared the loss activity of both catalyst, the metal leaching was mainly responsible for this negative effect on activity. It was possible that the N doping is helpful to stabilize metal on the support [38]. This stabilizing phenomenon can also be partly elucidated by the higher reduction temperature of Ru-Ni-AC/N than Ru-Ni-AC in H₂-TPR (Fig. 5) analyses.

3.4. Optimization of reaction conditions

The yield of aromatics is related to the amount of desorbed hydrogen which be greatly affected by the composition and distribution of the loaded active metals[37], thus an appropriate Ru/Ni ratio is important for the catalytic system. Fig. 7 displayed the influence of Ru and Ni contents on catalysts performances. The results showed that a higher Ru content leaded to a more active catalyst when Ni content was held constant at 5 wt.% (Fig. 7a). 1.5 wt.% of Ru with 10 wt.% of Ni was found to be the optimal combination, obtaining 83% of conversion and 79% of selectivity (Fig. 7b).

The effect of H₂ pressure on the hydrogenolysis reaction was shown in Fig. 8. With the H₂ pressure increasing from 0.5 MPa to 2 MPa, the conversion of guaiacol raised from 10% to 95%, but the

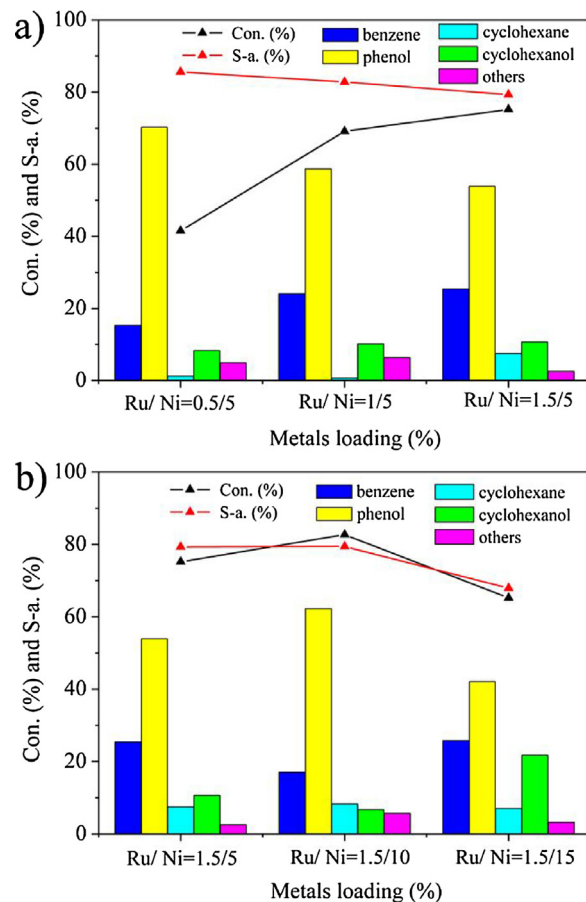


Fig. 7. The effect of a) Ru and b) Ni loading on guaiacol conversion. Reaction conditions: guaiacol 6.0 mmol, catalyst 0.1 g, H₂O 35 mL, 230 °C, H₂ 1.0 MPa, 4 h.

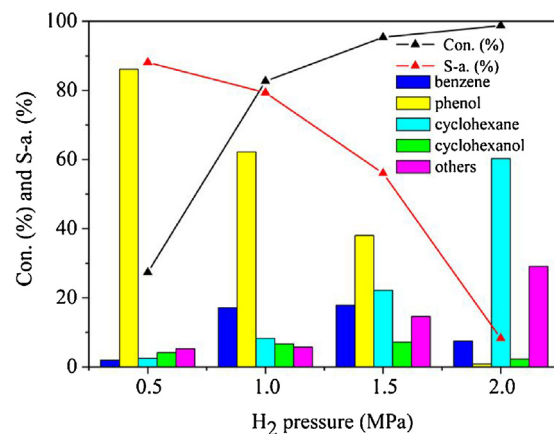


Fig. 8. The effect of H₂ pressure on guaiacol conversion. Reaction conditions: guaiacol 6.0 mmol, 1.5%Ru-10%Ni-AC/N 0.1 g, H₂O 35 mL, 230 °C, 4 h.

selectivity to aromatics was declined because of the further hydrogenation of benzene ring. The maximum yield of aromatics was achieved with H₂ pressure of 1.0 MPa, and phenol was the major product.

The influence of reaction temperature was shown in Fig. 9. Low temperature (180 °C and 200 °C) was favorable for the hydrogenation of benzene rings in producing cyclohexanol, while high temperature (230 °C and 250 °C) was good for hydrogenolysis of guaiacol to form benzene and phenol. The optimized reaction temperature was 250 °C with a conversion of 92% and selectivity to aromatics of 84%. With a decrease in the reaction temperature,

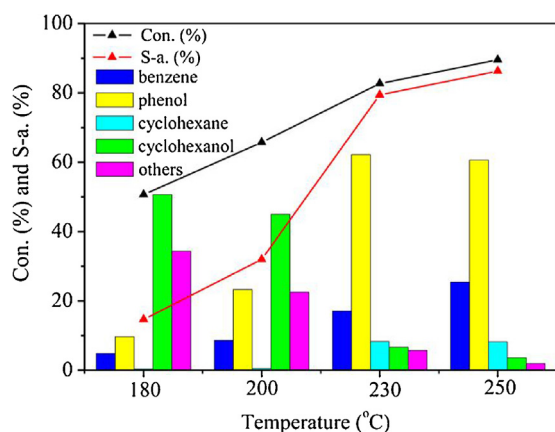


Fig. 9. The effect of reaction temperature on guaiacol conversion. Reaction conditions: guaiacol 6.0 mmol, 1.5%Ru-10%Ni-AC/N 0.1 g, H₂O 35 mL, H₂ 1.0 MPa, 4 h.

hydrogen concentration in the water became higher, which was conducive to create spillover hydrogen on the catalyst surface that enhanced the selectivity of excessive hydrogenation products (cyclohexanol and cyclohexane) [39].

As shown in Fig. 10, the product distribution and conversion depended heavily on the solvent. Water, methanol, ethanol, *n*-dodecane and decalin were chosen as reaction media and water was proved to be the suitable reaction solvent. When methanol and ethanol was used, much lower catalytic conversion (<20%) was obtained. Such oxygen-containing solvents could occupy the active sites of the catalysts, which would significantly affect the guaiacol conversion [40]. It was also reported by Wang and coworkers [41] that methanol and ethanol was protic solvents, displayed high polarity and Lewis basicity as indicated by the highest values of donor number (DN > 100 kJ mol⁻¹), which markedly reduced

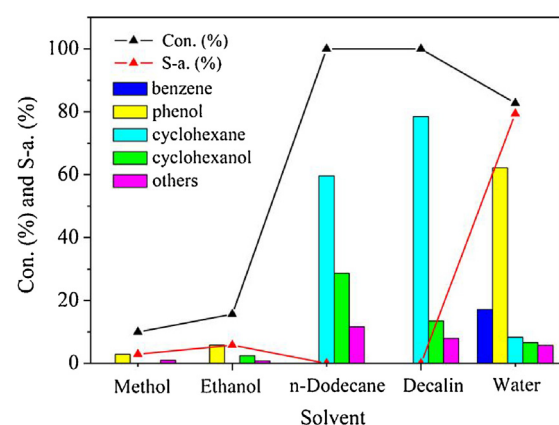


Fig. 10. The effect of solvent on guaiacol conversion. Reaction conditions: guaiacol 6.0 mmol, 1.5%Ru-10%Ni-AC/N 0.1 g, solvent 35 mL, 230 °C, H₂ 1.0 MPa, 4 h.

the catalytic activity towards hydrogenolysis of phenols. Full conversion (100%) was achieved by using decalin and *n*-dodecane as solvent media, but the selectivity to aromatics is quite low. As aprotic nonpolar solvents, they showed no Lewis basicity (DN = 0), which made cycloalkanes as their desired products [41]. when water was used as solvent, 79% of selectivity and 83% of conversion were obtained because the H⁺ ion created from water under such hydrothermal conditions could act as the acid and thus accelerated the hydrogenolysis rate of guaiacol [42].

3.5. Study the selectivity of catalysts

In order to figure out the reason of high aromatics selectivity of Ru-Ni-AC/N, benzene and phenol, two of the objected products, were also selected to react with the three catalysts

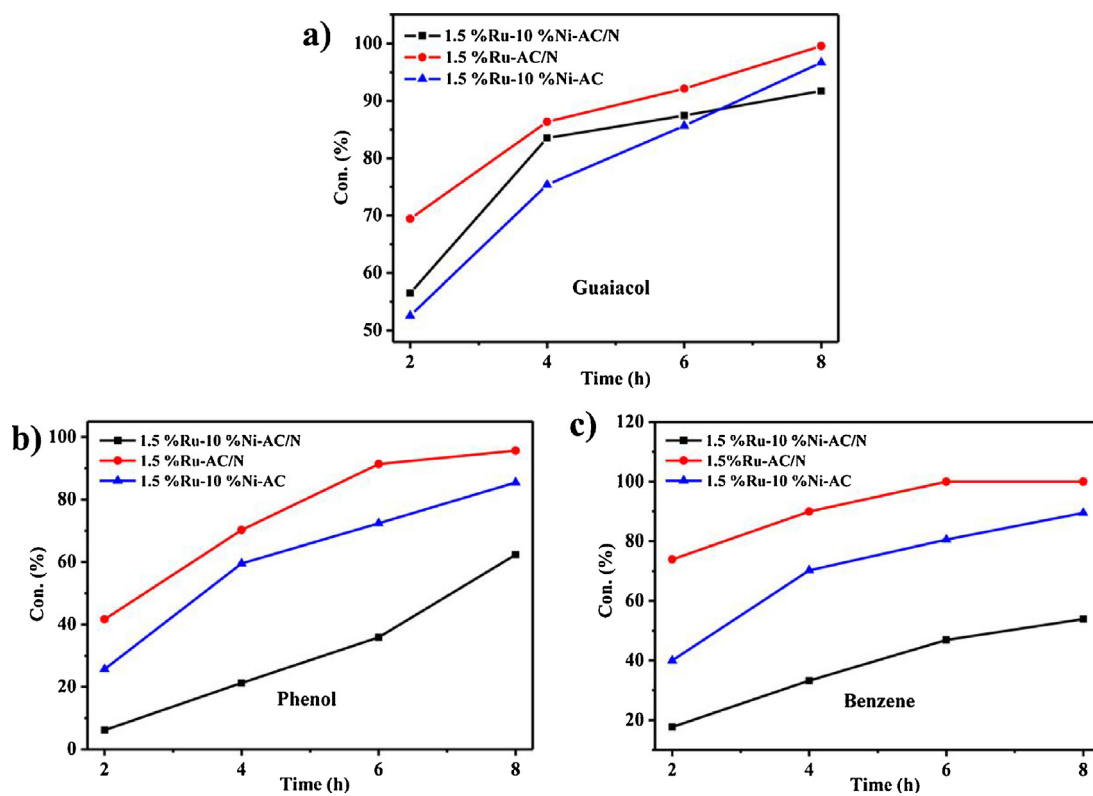


Fig. 11. The conversion of a) guaiacol, b) phenol and c) benzene depended on the catalysts used with the reaction times. Reaction conditions: substrates 6.0 mmol, catalysts 0.1 g, H₂O 35 mL, 230 °C, H₂ 1.0 MPa.

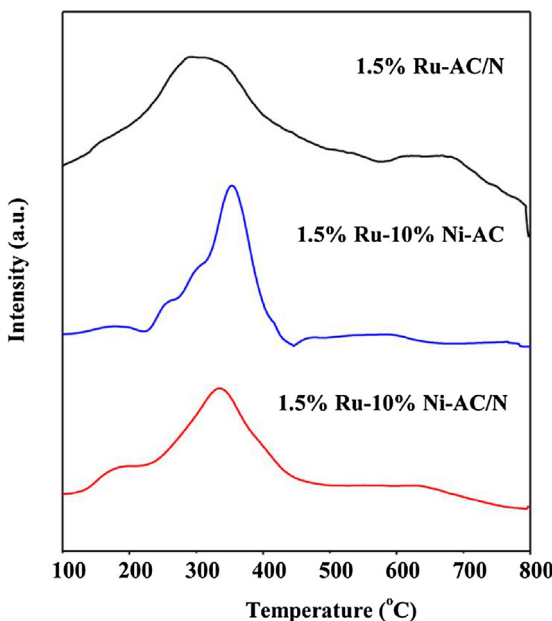


Fig. 12. H_2 -TPD spectra of reduced 1.5%Ru-10%Ni-AC/N, 1.5%Ru-AC/N and 1.5%Ru-10%Ni-AC catalysts.

Table 3
Metal leaching from the hydrogenolysis reaction as measured by ICP-MS.^a

Catalyst	Cycle	Ru concentration(ug/ml)	Ni concentration(mg/ml)
1%Ru-5%Ni-AC	1	14.27	13.04
1%Ru-5%Ni-AC/N	1	2.72	4.79
1%Ru-5%Ni-AC	2	14.80	6.65
1%Ru-5%Ni-AC/N	2	2.05	3.08
1%Ru-5%Ni-AC	3	6.23	4.11
1%Ru-5%Ni-AC/N	3	1.66	1.56

^a Reaction conditions: guaiacol 6.0 mmol, 1%Ru-5%Ni-AC/N 0.1 g, H_2O 35 mL, 230 °C, H_2 1.0 MPa, 4 h.

(Ru-Ni-AC/N, Ru-AC/N, Ru-Ni-AC) under the optimized reaction conditions (Fig. 11). In the first 6 h, 1.5%Ru-10%Ni-AC/N achieved a moderate conversion for guaiacol but the lowest conversion for phenol or benzene. It demonstrated that the intermediate products of guaiacol (phenol or benzene) were not reacted fiercely in the optimized catalytic system, leading a high selectivity towards aromatics.

H_2 -TPD was performed to study the hydrogen adsorption ability of the three catalysts (Fig. 12) since hydrogen adsorption ability on the catalyst surface is vital for lignin model compounds conversion [43]. The peak below 600 °C was related to hydrogen desorption and peak above 600 °C referred to the gasification of carbon supports

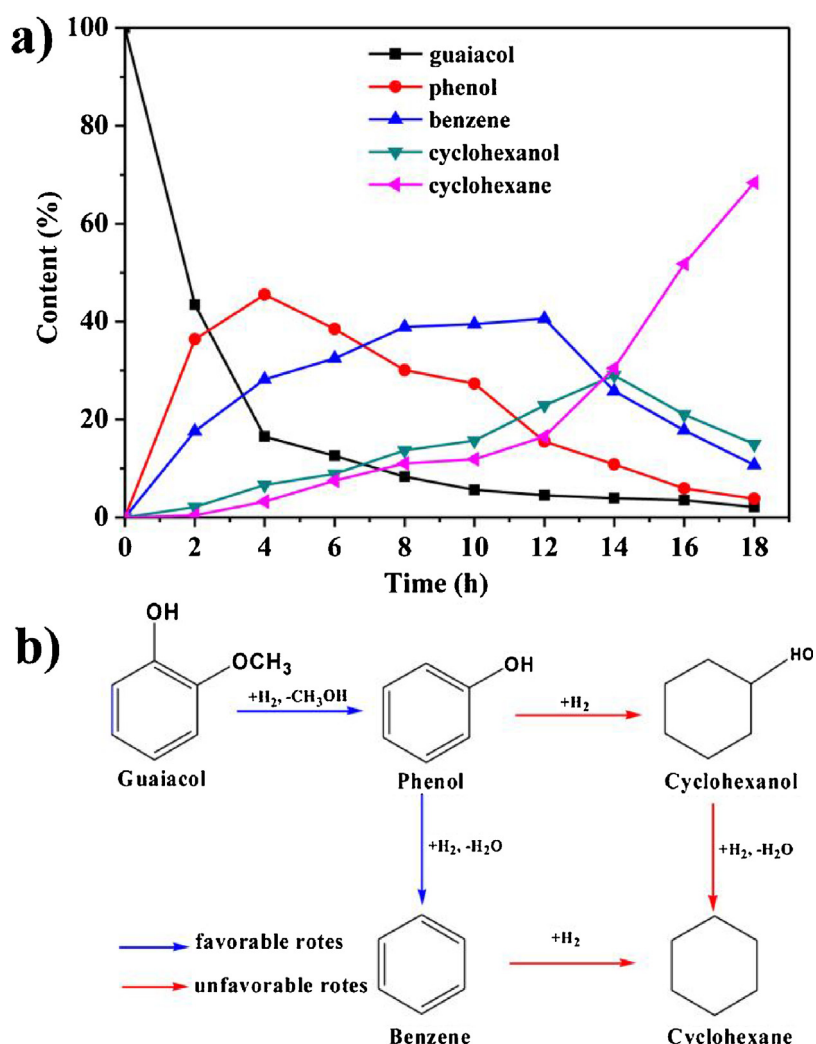


Fig. 13. a) Evolution of reactant and product concentrations with reaction time and b) possible reaction pathways of Ru-Ni-AC/N for hydrogenolysis guaiacol. Reaction conditions: guaiacol 6.0 mmol, 1.5%Ru-10%Ni-AC/N 0.1 g, H_2O 35 mL, 230 °C, H_2 1.0 MPa.

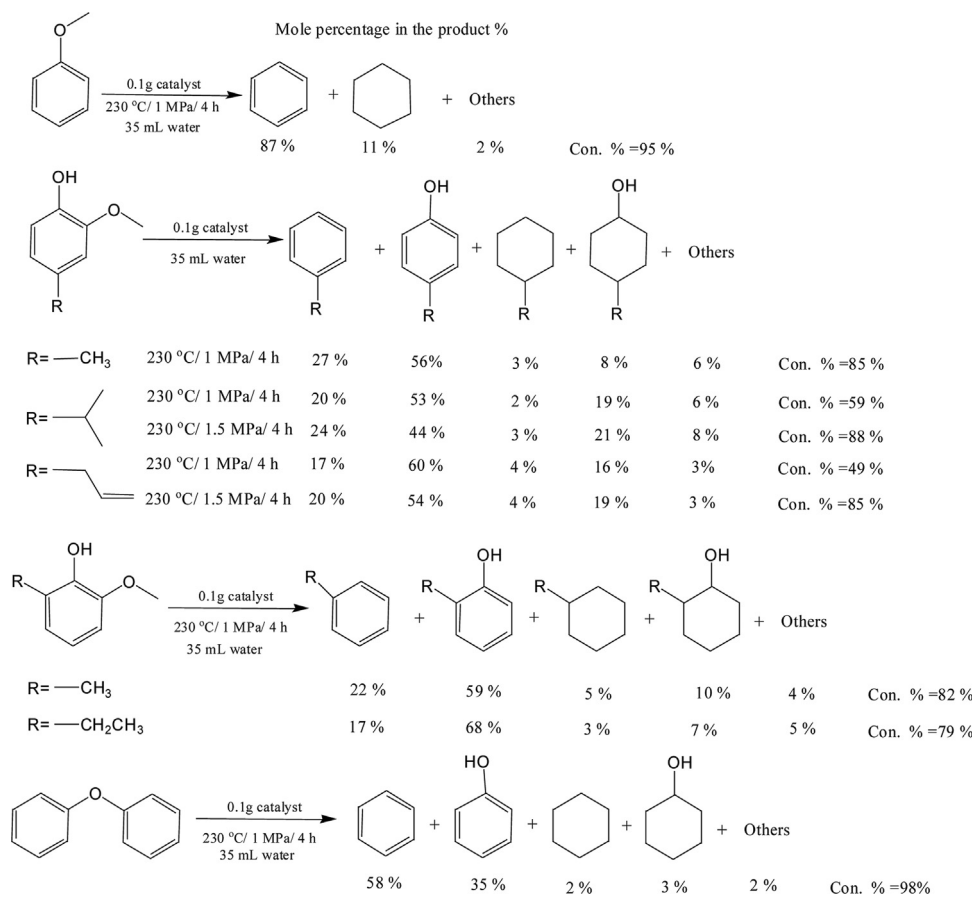


Fig. 14. Hydrogenolysis of other lignin model compounds with 1.5% Ru-10%Ni-AC/N catalyst. The substrate was 6.0 mmol for each reaction.

Table 4

H₂-TPD results of reduced 1.5%Ru-10%Ni-AC/N, 1.5%Ru-AC/N, 1.5%Ru-10%Ni-AC catalysts.^a

Catalyst	Amount of desorbed hydrogen (umol/g)
1.5%Ru-AC/N	98.2
1.5%Ru-10%Ni-AC	65.3
1.5%Ru-10%Ni-AC/N	46.5

^a Calculated with peak below 600 °C.

[44]. As listed in Table 4, the amount of desorbed hydrogen (the area of peak below 600 °C) in the catalysts were decreased in the order of 1.5%Ru-AC/N > 1.5%Ru-10%Ni-AC > 1.5%Ru-10%Ni-AC/N. This trend was in inverse proportion to the trend of activity for those catalysts in benzene and phenol conversion. It is known that the strong hydrogen adsorption ability of Ru causes hydrogenation of C=C bond in aromatic ring [45]. The introduce of inactive Ni and high charged N-groups could decreases the hydrogen uptake of Ru-Ni-AC/N and thus provide an inhibition for hydrogenation of aromatic rings. The highest hydrogen adsorption ability of Ru-AC/N causes a very high conversion of guaiacol, while the major products were cyclohexane and cyclohexanol. Hydrogenolysis of C_{Ar}-OCH₃ bond was the main reaction pathway with Ru-Ni-AC/N and Ru-Ni-AC catalyst for guaiacol conversion. Although the hydrogen adsorption of Ru-Ni-AC/N was lower than Ru-Ni-AC catalyst, the strong attraction effect to —OCH₃ group [46] and improved hydrogenolysis ability [38] caused by electron rich N atoms could speed up its conversion in the first 6 h. From the above results, the relatively low adsorption ability of hydrogen on the catalyst was a critical factor to selectively produce aromatics for the optimized catalyst.

3.6. Reaction pathways

A set of hydrogenolysis reactions with varies reaction time was conducted to obtain more information on kinetics (Fig. 13).

According to the results, guaiacol was decreased rapidly, while phenol was increased to its maximum in the first 4 h, which illustrated that the demethoxylation of guaiacol was the first step for the hydrogenolysis reaction. Subsequently, the content of phenol began to decrease with the reason that dehydroxylation and hydrosaturation of the aromatic structure proceeded concurrently. The amount of benzene was increased gradually as the reaction proceeded (in 12 h), and so did the ring hydrogenation products (cyclohexanol and cyclohexane). Cyclohexanol reached its maximum in 14 h and then decreased, while the cyclohexane kept increasing until the reaction finished (18 h), resulting from the dehydroxylation of cyclohexanol and hydrosaturation of benzene. Thus, a possible mechanism of Ru-Ni-AC/N for hydrogenolysis of guaiacol was proposed as following: phenol was the major intermediate formed through demethoxylation of guaiacol; the conversion of phenol proceeded in two reaction pathways: 1) dehydroxylation of phenol to form benzene (favorable route) and then hydrogenated to cyclohexane (unfavorable route); 2) hydrogenation of phenol via ring saturation to form cyclohexanol (unfavorable route) and then to cyclohexane (unfavorable route).

3.7. Hydrogenolysis of other lignin model phenols

In order to explore the application scope of Ru-Ni-AC/N catalyst, it was used in the hydrogenolysis of other monomeric phenols which commonly existed in the lignin phenolic mixture (Fig. 14).

For anisole, Ru-Ni-AC/N catalyst can effectively cleavage C_{Ar}—O bond to make benzene the major product. Comparable conversion (~80%) and aromatics selectivity (~80%) was obtained for hydrogenolysis of methyl- or ethyl- guaiacol. The side chains increases the difficulty for hydrogenolysis reaction, to achieve a satisfactory conversion of eugenol and isopropyl guaiacol, higher H₂ pressure (1.5 MPa) were needed. Eugenol and propyl guaiacol showed well conversion of ~85% and aromatics selectivity of ~70%. Ru-Ni-AC/N catalyst also exhibited an excellent activity (>90%) for transforming diphenyl ether into aromatic compounds.

4. Conclusion

In summary, the catalyst of bimetallic Ru-Ni supported on nitrogen-doped activated carbon (Ru-Ni-AC/N) is an active, stable and effective catalyst for the hydrogenolysis of lignin model compounds to aromatics under mild reaction conditions. HRTEM, XPS and H₂-TPR demonstrated the strong synergistic effect existed between Ru and Ni in bimetallic catalyst contributes to its improved hydrogenolysis activity. The introduction of electron rich N atoms onto AC not only leaded to an interaction effect between supports and metals but also retained the metal particles, which significantly enhanced its aromatics selectivity and catalyst stability. Furthermore, a moderate metals content (1.5%Ru-10%Ni), high temperature (>230 °C) and low H₂ pressure (1 MPa) were also found to be benefit to produce aromatics. The catalyst also showed good activity in the hydrogenolysis of other lignin model compounds.

Acknowledgements

Financial support from The Boeing Company (Project Agreement #2015-159) is greatly acknowledged. We also thank the National Natural Science Foundation of China (21273260 and 21433001), the Shandong Provincial Natural Science Foundation for Distinguished Young Scholar (JQ201305), the Youth Innovation Promotion Association CAS (2015168) and the Young Taishan Scholars Program of Shandong Province (tsqn20161052) for financial support.

References

- [1] S. Pichaikan, P. Arumugam, *Green Chem.* 18 (2016) 2888–2899.
- [2] Z. Luo, Y. Wang, M. He, C. Zhao, *Green Chem.* 18 (2016) 433–441.
- [3] A.G. Sergeev, J.D. Webb, J.F. Hartwig, *J. Am. Chem. Soc.* 134 (2012) 20226–20229.
- [4] C. Diaz-Urrutia, B.B. Hurisso, P.M.P. Gauthier, B. Sedai, R.D. Singer, R.T. Baker, *J. Mol. Catal. A-Chem.* 423 (2016) 414–422.
- [5] M. Hellinger, H.W.P. Carvalho, S. Baier, D. Wang, W. Kleist, J.-D. Grunwaldt, *Appl. Catal. A-Gen.* 490 (2015) 181–192.
- [6] M.V. Bykova, D.Y. Ermakov, S.A. Khromova, A.A. Smirnov, M.Y. Lebedev, V.A. Yakovlev, *Catal. Today* 220 (2014) 21–31.
- [7] J.E. Peters, J.R. Carpenter, D.C. Dayton, *Energy Fuel* 29 (2015) 909–916.
- [8] W. Wang, L. Li, K. Wu, G. Zhu, S. Tan, Y. Liua, Y. Yang, *RSC Adv.* 6 (2016) 31265–31271.
- [9] M. Rubes, J. He, P. Nachtigall, O. Bludsky, *J. Mol. Catal. A-Chem.* 423 (2016) 300–307.
- [10] B. Guvenatam, O. Kursun, E.H.J. Heeres, E.A. Pidko, E.J.M. Hensen, *Catal. Today* 233 (2014) 83–91.
- [11] S. Oh, H. Hwang, H.S. Choi, J.W. Choi, *Fuel* 153 (2015) 535–543.
- [12] R.H. Bowker, M.C. Smith, M.L. Pease, K.M. Slenkamp, L. Kovarik, M.E. Bussell, *ACS Catal.* 1 (2011) 917–922.
- [13] J.-S. Moon, Y.-K. Lee, *Top. Catal.* 58 (2015) 211–218.
- [14] J. He, C. Zhao, D. Mei, J.A. Lercher, *J. Catal.* 309 (2014) 280–290.
- [15] C. Bosagli, K. Raffelt, T.A. Zevaco, W. Olbrich, T.N. Otto, J. Sauer, J.-D. Grunwaldt, *Biomass Bioenerg.* 83 (2015) 525–538.
- [16] Y. Hong, H. Zhang, J. Sun, K.M. Ayman, A.J.R. Hensley, M. Gu, M.H. Engelhard, J.-S. McEwen, Y. Wang, *ACS Catal.* 4 (2014) 3335–3345.
- [17] J. Sun, A.M. Karim, H. Zhang, L. Kovarik, X.S. Li, A.J. Hensley, J.-S. McEwen, Y. Wang, *J. Catal.* 306 (2013) 47–57.
- [18] R.J. White, R. Luque, V.L. Budarin, J.H. Clark, D.J. Macquarrie, *Chem. Soc. Rev.* 38 (2009) 481–494.
- [19] Z. Li, J. Li, J. Liu, Z. Zhao, C. Xia, F. Li, *Chemcatchem* 6 (2014) 1333–1339.
- [20] X. Xu, Y. Li, Y. Gong, P. Zhang, H. Li, Y. Wang, *J. Am. Chem. Soc.* 134 (2012) 16987–16990.
- [21] Q. Liu, G. Xu, X. Wang, X. Mu, *Green Chem.* 18 (2016) 2811–2818.
- [22] S.M.S. Kumar, J.S. Herrero, S. Irusta, K. Scott, *J. Electroanal. Chem.* 647 (2010) 211–221.
- [23] Y. Tian, Y.-Y. Cao, F. Pang, G.-q. Chen, X. Zhang, *RSC Adv.* 4 (2014) 43204–43211.
- [24] Z. Dong, C. Dong, Y. Liu, X. Le, Z. Jin, J. Ma, *Chem. Eng. J.* 270 (2015) 215–222.
- [25] L. Zhu, S. Shan, V. Petkov, W. Hu, A. Krone, J. Zheng, C. Yu, N. Zhang, Y. Li, R. Luque, C.-J. Zhong, H. Ye, Z. Yang, B.H. Chen, *J. Mater. Chem. A* 5 (2017) 7869–7875.
- [26] L.S. Ribeiro, J.J. Delgado, J.J.M. Orfao, M.F.R. Pereira, *Appl. Catal. B-Environ.* 217 (2017) 265–274.
- [27] F. Morales-Cano, L.F. Lundsgaard, R.R. Tiruvalam, H. Falsig, M.S. Skjøth-Rasmussen, *Appl. Catal. A-Gen.* 498 (2015) 117–125.
- [28] D.J. Morgan, *Surf. Interface Anal.* 47 (2015) 1072–1079.
- [29] Y. Wang, S. De, N. Yan, *Chem. Commun.* 52 (2016) 6210–6224.
- [30] Q. Zhang, X.-P. Wu, Y. Li, R. Chai, G. Zhao, C. Wang, X.-Q. Gong, Y. Liu, Y. Lu, *ACS Catal.* 6 (2016) 6236–6245.
- [31] J. Li, J.-I. Liu, H.-j. Zhou, Y. Fu, *Chemsuschem* 9 (2016) 1339–1347.
- [32] X. Cui, A.-E. Sürküs, K. Junge, C. Topf, J. Radnik, C. Kreyenschulte, M. Beller, *Nat. Commun.* 7 (2016).
- [33] W. Zhao, W. Li, J. Zhang, *Catal. Sci. Technol.* 6 (2016) 1402–1409.
- [34] S. De, J. Zhang, R. Luque, N. Yan, *Energ. Environ. Sci.* 9 (2016) 3314–3347.
- [35] J. Zhang, M. Ibrahim, V. Colliere, H. Asakura, T. Tanaka, K. Teramura, K. Philippot, N. Yan, *J. Mol. Catal. A-Chem.* 422 (2016) 188–197.
- [36] D.P. Serrano, J.M. Escola, L. Briones, S. Medina, A. Martinez, *Fuel* 144 (2015) 287–294.
- [37] J.K. Kim, J.K. Lee, K.H. Kang, J.W. Lee, I.K. Song, *J. Mol. Catal. A-Chem.* 410 (2015) 184–192.
- [38] H. Jiang, X. Yu, R. Nie, X. Lu, D. Zhou, Q. Xia, *Appl. Catal. A-Gen.* 520 (2016) 73–81.
- [39] H. Shahaghian, P.S. Rezaei, W.M.A.W. Daud, *RSC Adv.* 5 (2015) 33990–33998.
- [40] M. Hellinger, H.W.P. de Carvalho, S. Baier, L. Gharnati, J.D. Grunwaldt, *Chem. Chem. Ing. Tech.* 87 (2015) 1771–1780.
- [41] X. Wang, R. Rinaldi, *Chemsuschem* 5 (2012) 1455–1466.
- [42] M.-Y. Chen, Y.-B. Huang, H. Pang, X.-X. Liu, Y. Fu, *Green Chem.* 17 (2015) 1710–1717.
- [43] M.W. Jarvis, J.W. Daily, H.-H. Carstensen, A.M. Dean, S. Sharma, D.C. Dayton, D.J. Robichaud, M.R. Nimlos, *J. Phys. Chem. A* 115 (2011) 428–438.
- [44] X. Dong, H.B. Zhang, G.D. Lin, Y.Z. Yuan, K.R. Tsai, *Catal. Lett.* 85 (2003) 237–246.
- [45] J.G. Zhang, J. Teo, X. Chen, H. Asakura, T. Tanaka, K. Teramura, N. Yan, *ACS Catal.* 4 (2014) 1574–1583.
- [46] A. Thomas, A. Fischer, F. Goettmann, M. Antonietti, J.-O. Mueller, R. Schloegl, J.M. Carlsson, *J. Mater. Chem.* 18 (2008) 4893–4908.